Published in final edited form as:
Nature. 2008 November 13; 456(7219): 255–258. doi:10.1038/nature07380.

Stereocilin-deficient mice reveal the origin of cochlear waveform distortions

Elisabeth Verpy[1,2,3,4], **Dominique Weil**[1,2,3,4,*], **Michel Leibovici**[1,2,3,4,*], **Richard J. Goodyear**[5], **Ghislaine Hamard**[6], **Carine Houdon**[1,2,3,4], **Gaelle M. Lefèvre**[1,2,3,4], **Jean-Pierre Hardelin**[1,2,3,4], **Guy P. Richardson**[5], **Paul Avan**[7,#], and **Christine Petit**[1,2,3,4,#]

[1]Institut Pasteur, Unité de Génétique et Physiologie de l'Audition, F75015 Paris, France.

[2]Inserm UMRS 587, F75015 Paris, France.

[3]Collège de France, F75015 Paris, France.

[4]Université Pierre et Marie Curie, F75015 Paris, France.

[5]University of Sussex, School of Life Sciences, Falmer, Brighton BN1 9QG, UK.

[6]Institut Cochin, Plate-Forme de Recombinaison Homologue, F75014 Paris, France.

[7]Université d'Auvergne, Laboratoire de Biophysique Sensorielle, F63001 Clermont-Ferrand, France.

Abstract

Although the cochlea is an amplifier and a remarkably sensitive and finely tuned detector of sounds, it also produces conspicuous mechanical and electrical waveform distortions[1]. These distortions reflect non-linear mechanical interactions within the cochlea. By allowing one tone to suppress another (masking effect), they contribute to speech intelligibility[2]. Tones can also combine to produce sounds with frequencies not present in the acoustic stimulus[3]. These sounds compose the otoacoustic emissions that are extensively used to screen hearing in newborns. As both cochlear amplification and distortion originate from the outer hair cells, one of the two types of sensory receptor cells, it has been speculated that they stem from a common mechanism. Here, the non-linearity underlying cochlear waveform distortions is shown to rely on the presence of stereocilin, a protein defective in a recessive form of human deafness[4]. Stereocilin was detected in association with horizontal top connectors[5-7], lateral links that join adjacent stereocilia within the outer hair cell's hair bundle, and these links were absent in stereocilin-null mutant mice. These mice become progressively deaf. At the onset of hearing, however, their cochlear sensitivity and frequency tuning were almost normal, although masking was much reduced and both acoustic and electrical waveform distortions were completely lacking. From this unique functional situation, we conclude that the main source of cochlear waveform distortions is a deflection-dependent hair

Correspondence and requests for material should be addressed to C.P. (cpetit@pasteur.fr) or E.V. (everpy@pasteur.fr)..
*These authors contributed equally to the work.
#These authors contributed equally to the work.

Author Contributions C.P. and P.A. contributed equally as co-senior authors. D.W. and M. L. are co-second authors. D.W. and G.H. produced the *Strc* knockout mice. P.A. conducted the auditory tests. M.L. performed the SEM experiments on wild-type, *Strc*$^{-/-}$ and *Tecta*$^{\Delta ENT/\Delta ENT}$ mice, with C.H.'s help. G.M.L. carried out the SEM experiment on the *Ush1c*$^{-/-}$ mouse. E.V. performed the IF studies with C.H.'s help and RT-PCR analysis. G.P.R. and R.J.G carried out the TEM analysis. E.V. supervised the stereocilin expression studies and the characterization of the morphological anomalies in the *Strc* knockout mice. C.P. supervised the whole project with G.P.R.'s help and in collaboration with P.A for the physiological studies. E.V., J.-P.H., G.P.R, P.A., and C.P. prepared the manuscript.

Supplementary Information is linked to the online version of the paper at www.nature.com/nature.

Europe PMC Funders Author Manuscripts

bundle stiffness resulting from constraints imposed by the horizontal top connectors, and not from the intrinsic non-linear behaviour of the mechanoelectrical transducer channel.

The cochlea is a highly-sensitive and sharply-tuned sound detector. It contains two types of sensory cells: outer hair cells (OHCs) that locally amplify and sharpen sound-induced mechanical stimulation of the cochlear partition, and inner hair cells (IHCs) that transmit sensory information to the brain. OHCs have been proposed to supply forces for amplification by changing the length and stiffness of their lateral wall in response to changes in membrane potential (a process known as electromotility)[8-11], or by active movement of their apically-located mechanosensory hair bundle[12,13]. The OHC hair bundle is composed of actin-filled stereocilia arrayed in three rows of increasing height. The tallest stereocilia are embedded in the tectorial membrane, an acellular gel overlying the sensory epithelium. The stereocilia are coupled together by the tip link, that extends from the tip of a stereocilium to the side of the adjacent taller one and may gate the mechanoelectrical transducer (MET) channels[12], and by zipper-like horizontal top connectors that join the upper parts of adjacent stereocilia within and between rows[5-7] (supplementary Fig. 1a).

Mutations in the gene encoding stereocilin (supplementary Fig. 1b), a protein of the hair bundle, cause prelingual hearing impairment in man[4]. We engineered mutant mice with a frame-shifting deletion in the stereocilin gene (supplementary Fig. 2). In postnatal day 60 (P60) stereocilin-null (*Strc*$^{-/-}$) mice, auditory brainstem responses to tones in the 5-40 kHz frequency range showed increased thresholds, up to 60 dB (data not shown). As these threshold shifts suggested a possible failure of the cochlear amplifier[14,15], we studied cochlear sensitivity, frequency selectivity, as well as waveform distortions and masking interactions among spectral components of a complex sound[15], all ascribed to the functioning of the OHCs.

The signal recorded by a round-window electrode contains the compound action potential (CAP) from the cochlear nerve, representing synchronous neural activity in response to short tone bursts. CAP thresholds, by assessing cochlear sensitivity, allow estimation of amplification due to OHCs, normally ~60 dB at frequencies > 10 kHz[16]. P14-15 mice still have immature CAP thresholds (Fig. 1a vs 1b), but their mechanical and electrical cochlear responses are adult-like (see Figs 1d, 1e, 2a), indicating the immaturity of their CAP thresholds is likely to be neural in origin. At P14, the difference between CAP thresholds in *Strc*$^{-/-}$ mice and those of *Strc*$^{+/+}$ mice was not statistically significant, less than 10 dB on average in the 5-40 kHz range (Fig. 1a, supplementary Fig. 3). From P15 on, progressive hearing loss appeared in *Strc*$^{-/-}$ mice, increasing from a flat 25 dB to a ~60-dB ceiling above 10 kHz at P60 (Fig. 1b, supplementary Fig. 3).

The round-window electrode also collects the cochlear microphonic potential (CM), a phasic response reflecting MET currents from basal-coil OHCs. As low-frequency tones are not amplified by basal-coil OHCs, the amplitude of the CM response to these tones is proportional to the number of functional MET channels[17]. This number gradually decreased from P15 to P60 in *Strc*$^{-/-}$ mice (Fig. 1c). Models of active OHC operation (supplementary Fig. 4) predict how much gain the residual active MET channels would generate[17]. A statistically significant difference was not found between the predicted and observed auditory thresholds (Fig. 1c), which suggests that decreased number of functional MET channels in OHCs accounts for the increased CAP thresholds in *Strc*$^{-/-}$ mice.

How well OHCs determine frequency selectivity, a task dependent on amplification, can be addressed by measuring how a continuous masker tone at varying frequency and level affects the CAP response to a test tone-burst presented simultaneously and just above threshold[18]. Masking occurs when the masker enters the frequency band of the cochlear

Europe PMC Funders Author Manuscripts

filter centred on the test tone. We studied masking at 10 kHz (Fig. 1d,e) and 20 kHz (not shown). In P14 *Strc*$^{-/-}$ mice, CAP tuning curves revealed the persistence of fine frequency selectivity, as the quality factor of tuning, $Q_{10\ dB}$, remained similar to that of controls. CAP tuning curves also provide information on the strength of masking: the more upshifted their tip relative to the test tone level, the weaker the masking. Masking was weakened in P14 *Strc*$^{-/-}$ mice (Fig. 1d). Despite similar probe-tone levels, high-frequency maskers had to be >20 dB louder than in controls to provide the same CAP decrease. Simultaneous masking is due to two mechanisms[2,19]. One is neuronal and due to the masker producing action potentials that place neurons in the refractory period, and therefore unable to respond to the test tone (line-busy masking). Since stereocilin was not detected in the cochlear ganglion neurons (data not shown), this process should be preserved in *Strc*$^{-/-}$ mice. The other mechanism, suppressive masking, is due to non-linear interactions between masker and test tones decreasing the mechanical response to the test tone. This suppressive masking shows up in the basilar membrane mechanical response[18]. Of note, the extent of the decrease of the masking strength observed in *Strc*$^{-/-}$ mice is reminiscent of the suppression of the chinchilla basilar membrane motion induced by a high- or low-frequency tone at levels similar to those used here[20]. This suggests *Strc*$^{-/-}$ mice totally lack suppressive interactions, the persisting masking thus being due to the line-busy mechanism only.

The mechanical non-linearity that contributes to masking may also distort acoustic waveforms, so that in response to two-tone stimuli (frequencies f_1, f_2), distortion-product otoacoustic emissions (DPOAEs) at intermodulation frequencies ($2f_1$-f_2, f_2-f_1, etc) are propagated backward and detected as combination tones in the ear canal[21,22]. From P14 on, control mice presented DPOAE components well above the noise floor. In contrast, *Strc*$^{-/-}$ mice had no detectable DPOAEs up to 80 dB SPL (Fig. 2a).

The complete absence of suppressive masking and DPOAEs in *Strc*$^{-/-}$ mice as early as P14, despite normal hearing thresholds and tuning curves, prompted a search for electrical distortion products. These show up as a levelling out of the CM waveforms that originate from MET currents through OHCs (Fig. 2b). In response to tonal stimuli at frequency f in P14 control mice, CM exhibited harmonics 2f and 3f at about −30 dB relative to the levels of the fundamental frequency (not shown). For two-tone stimuli with neighbouring frequencies f_1 and f_2, P14 control mice exhibited CM waveforms with multiple inter-modulation components reaching −12 to −15 dB relative to stimulus levels (Fig. 2b). Finally, when an infrasound bias (<0.6 kHz) was mixed with an audible frequency (5-10 kHz), the CM in P14 control mice showed periodic suppressive amplitude modulation, even for biasing levels as low as 85 dB SPL (Fig. 2c). In contrast, P14 *Strc*$^{-/-}$ mice showed none of these CM waveform distortions whatever the intensity of the acoustic stimulation up to 100 dB SPL (Fig. 2b,c). Histological examination of the cochlea in P14 *Strc*$^{-/-}$ mice did not reveal any gross structural anomalies. Scanning electron microscopy showed the tectorial membrane extended across the sensory epithelium, as in wild-type mice. Hair-bundle imprints corresponding to the anchoring points of the tallest OHC stereocilia[23] were, however, not observed (not shown). Nonetheless, CM waveforms had the same phase relative to sound in *Strc*$^{-/-}$ and control mice (supplementary Fig. 5) indicating that, in both cases, OHCs were driven by the displacement of the cochlear partition, and not its velocity as they are in *Tecta*$^{\Delta ENT/\Delta ENT}$ mice, in which the tectorial membrane is detached from the sensory epithelium[24]. Strikingly, in all OHCs, but not in IHCs, the tops of the stereocilia rows were less clearly aligned in *Strc*$^{-/-}$ compared to *Strc*$^{+/+}$ mice (Fig. 3b). In keeping with the apparently loose connection between adjacent stereocilia, the horizontal top connectors that normally develop from P9 on and are fully mature at P14[7] could not be detected in P14 *Strc*$^{-/-}$ OHCs by scanning (Fig. 3d) and transmission (not shown) electron microscopy. By contrast, the tip links were still present (Fig. 3d).

The distribution of stereocilin was analysed in P14 wild-type mice, and compared to that in *Tecta*$^{\Delta ENT/\Delta ENT}$ mice[24]. Stereocilin was detected in the hair bundles of OHCs only. It was present in the distal regions of all stereocilia rows, in both wild-type and *Tecta*$^{\Delta ENT/\Delta ENT}$ mice (Fig. 4a and data not shown). Scanning immunoelectron microscopy revealed stereocilin was distributed in a ring around the tip of each stereocilium from the tallest row in the OHCs of wild-type mice, but not of *Tecta*$^{\Delta ENT/\Delta ENT}$ mice (Fig. 4b,c), suggesting stereocilin is involved in the contact these stereocilia establish with the tectorial membrane. In addition, stereocilin was detected between all OHC stereocilia, both in wild-type and *Tecta*$^{\Delta ENT/\Delta ENT}$ mice (Fig. 4b,c). The protein was found to be associated with the horizontal top connectors by transmission immunoelectron microscopy (Fig. 4d). In OHCs, these links are characterised by a central density (refs. 5-7 and supplementary Fig. 1a) that may be contributed by stereocilin, predicted to be an extracellular protein according to its amino-acid sequence.

The presence of DPOAEs in *Tecta*$^{\Delta ENT/\Delta ENT}$ mice[25] indicates the tectorial membrane is not essential for DPOAE production. The absence of all intermodulation and harmonic components in the responses of P14 *Strc*$^{-/-}$ mice, despite preserved amplification and tuning, thus suggests that their OHC hair bundles lack the very element at the origin of cochlear waveform distortions. This element is commonly thought to be the MET channel[16,26] for the following two reasons. Firstly, the MET current relates to hair bundle deflection via the Boltzmann's distribution of the MET channels' open probability[27]. This sigmoidal transfer function converts sinusoidal hair bundle deflection into distorted MET currents. Secondly, the thermodynamics of shuffling of the MET channels from open to closed states introduces a non-linear, deflection-dependent stiffness[16,28]. In *Strc*$^{-/-}$ mice, one might assume that the MET transfer function has become linear over the waveform-distortion-free 30-100 dB SPL range. The corollary of this, however, is a reduction of the energy difference between the open and closed states relative to the thermal energy kT[26] that would then prevent MET channels from operating normally, which they do in P14 *Strc*$^{-/-}$ mice. The non-linear source of all cochlear waveform distortions that also permits suppressive masking should thus come not from the intrinsic working properties of the MET channels, but from a non-conductive hair-bundle stiffness impinging the response of the MET channels. Being the missing structure in waveform-distortion-free *Strc*$^{-/-}$ mice, horizontal top connectors qualify as an important source of non-linear stiffness, either directly or indirectly by providing the necessary condition for another mechanical element to operate non-linearly. The bending of neighbouring stereocilia toward each other that is observed when stereocilin-associated lateral links extend further towards the stereocilia base in mouse models of Usher syndrome type I (data not shown and supplementary Fig. 6) supports the importance of these links in hair bundle non-conductive stiffness. The lateral links and pivots of OHC stereocilia are well-acknowledged contributors to the component of the hair bundle stiffness derived from the restoring force. Being reportedly large[13,27,29,30], this stiffness component would indeed provide a more suitable basis for the large waveform distortions and the strong suppressive masking observed in normal cochleae, than the conductive stiffness related to the MET channels.

METHODS SUMMARY

Production of Strc knockout mice (Supplementary Fig. 2)

Stereocilin knockout mice (*Strc*$^{tm1Ugds/tm1Ugds}$, referred to as *Strc*$^{-/-}$) were produced using the Cre-lox system. We engineered mice in which exons 2 and 3 of *Strc* were floxed (loxP-*Strc*). *Strc*$^{-/-}$ mice were obtained by crossing these mice with a transgenic mouse expressing the Cre recombinase early and ubiquitously.

Recordings of cochlear microphonics, compound action potentials, and otoacoustic emissions

An electrode was placed in the round-window niche of anaesthetised mice. The receptor currents of basal sensory cells and the synchronous activity of the cochlear nerve were recorded in response to tone-bursts and mixtures of tone-bursts and interfering tones. The sensitivity, frequency selectivity, susceptibility to masking and ability of waveforms to exhibit distortion were compared in *Strc*$^{-/-}$ vs *Strc*$^{+/+}$ mice. A miniature microphone probe in the external ear canal allowed combination tones in response to two-tone stimuli to be recorded as otoacoustic emissions.

Histological analysis and immunolocalisation

The morphology of the cochlear sensory epithelia was studied in *Strc*$^{+/+}$ and *Strc*$^{-/-}$ mice using scanning electron microscopy. For immunolocalisation of stereocilin, we used two affinity-purified polyclonal rabbit antibodies, anti-B and anti-D, raised against the synthetic peptides CFLSPEELQSLVPLSD (amino-acids 970-985) and EQLAYLSPEQRRAVA (amino-acids 1753-1767) derived from the mouse stereocilin sequence (AF375593), respectively (Supplementary Fig. 1b). The distribution of stereocilin was analysed using confocal immunofluorescence microscopy, scanning and transmission immunoelectron microscopy.

METHODS

Generation of Strc$^{tm1Ugds/tm1ugds}$ knockout mice (Supplementary Fig. 2)

We designed a targeting vector in which exons 2 and 3 of *Strc* and the hygromycin selection cassette were flanked with loxP sites. Electroporation of the linearised vector into CK 35 embryonic stem (ES) cells[31] (derived from a 129/Sv mouse embryo) plated on hygromycin selective medium resulted in approximately 300 recombinant ES cell clones, of which five were correctly targeted. Two independent recombinant ES cell lines carrying the floxed allele were selected and injected into C57BL/6J host blastocysts. Mating of male chimeras with C57BL/6J females produced heterozygous animals. Integration of the recombinant DNA construct was confirmed by Southern blot analysis and PCR amplification of genomic DNA extracted from mice's tails. For Southern blot analysis, genomic DNA was digested with *Bgl* II and transferred on Immobilon-NY+ (Millipore) membrane. The membrane was probed with a PCR-amplified fragment obtained by using primers 5′-GAGCTTCTGTCCAGTGATAGTTCAG-3′ and 5′-TGCTTAGGAAGCTTTCTGCAGCATGGG-3′. The PCR primers used to genotype the floxed *Strc* allele were HR (5′-TGGACGTAAACTCCTCTTCAGACC-3′), located in the hygromycin resistance gene, and *Strc*-R1 (5′-AGGCTGAGCCCACAGCACAAAG-3′), located in *Strc* intron 4 outside the targeting vector. Mice heterozygous for the floxed *Strc* allele were mated with the PGK-Cre^{m} transgenic mouse strain carrying the Cre recombinase gene driven by the early acting phosphoglycerate kinase-1 gene promoter[32]. Targeted deletion of exons 2 and 3 was confirmed by PCR analysis. Routine genotyping of animals for the *Strc*^{tm1Ugds} allele was carried out by two PCR amplifications, using forward primer *Strc*-F1 (5′-GGGCTCTGAGGAGGCTCTTTGGG-3′), located in exon 2, or *Strc*-F2 (5′-TGGGATTTGAACTCAGGTTGCTAGG-3′), located in intron 1, and reverse primer *Strc*-R2 (5′-CAGAGGCACACCTCTGCTCAGG-3′), located in exon 4. All studies were performed on mixed C57BL/6J-129/Sv genetic backgrounds.

For RT-PCR analysis, total RNA was isolated from single inner ears of P15 *Strc*$^{+/+}$, *Strc*$^{+/-}$ and *Strc*$^{-/-}$ mice, and forward primer 5′-53-TCTAGGCCCAGTGTGCACCT, located in exon 1, and reverse primer 5′-1192-GGCAGAGCAAGTAGATGGAGAAGTTGG, located in exon 4, were used for amplification. The amplicons were gel-purified and sequenced.

Recordings of cochlear microphonics (CM), compound action potentials (CAP) and distortion-product otoacoustic emissions (DPOAE)

For CAP, CM and DPOAE measurements, mice were anaesthetised with ketamine and levomepromazin. CAP and CM were collected between a silver electrode inserted in the round window niche and a vertex needle electrode. CAP and CM were evoked by tone-bursts (2-period rise–fall, 20-period plateau, repetition rate 20/s, sound level varying from 10 to 115 dB SPL in 5 dB steps). Masking and biasing were produced by adding to the test tone-burst a continuous pure tone with variable frequency and level (2.5 dB steps). The response from the electrodes was amplified (gain 5,000), filtered (0.02–30 kHz), digitally converted and averaged using a computerised data-acquisition system. Visual inspection was used to determine the CAP thresholds, or that CAP amplitude was halved in the presence of an increasingly loud masker. The DPOAE at frequency $2f_1$-f_2 was recorded in response to two equal level primary tones, f_1 and f_2, with $f_2/f_1 = 1.20$. Ear-canal sound pressure was amplified (x100) and averaged (0.5 s). The amplitudes of the DPOAE at $2f_1$-f_2 and of the background noise were extracted by Fast-Fourier transform. For CM waveform distortion measurements, the response from the electrode to one or two primary tones (levels ranging from 50 to100 dB SPL) was Fourier-transformed and analysed at harmonic and intermodulation frequencies. Statistical differences were evaluated using Student's t-test.

Antibodies and immunolabelling studies

Two rabbit immune sera, anti-B and anti-D, were produced against synthetic peptides B (NH_2-970-CFLSPEELQSLVPLSD-COOH) and D (NH_2-1753-EQLAYLSPEQRRAVA-COOH) derived from the mouse stereocilin amino-acid sequence, respectively (see supplementary Fig. 1b). The antibodies were affinity-purified on the corresponding peptides, and their specificity was verified by immunoblotting and immunostaining of transfected cells (Hela, Cos7, MDCK) producing full-length stereocilin, and by the loss of the inner ear immunolabelling in *Strc*$^{-/-}$ mice. Both antibodies gave similar staining patterns, but immunolabelling with anti-D required a pretreatment with methanol (Triton X-100 was ineffective), which precluded subsequent phalloidin staining. The results presented are those obtained with the anti-B antibody. For immunofluorescence detection, we used Alexa Fluor 488-conjugated goat anti-rabbit F(ab')$_2$ IgG fragment (1:800, Molecular Probes). Actin was labelled with TRITC-conjugated phalloidin (1 μg/ml, Sigma/Aldrich). Samples were processed as described[33], with the following modifications. Inner ears were fixed immediately upon removal by immersion in 4% paraformaldehyde in PBS pH 7.4 (PFA/PBS) for 30 min at room temperature. After three rinses in PBS, cochlear sensory areas were microdissected and re-fixed in PFA/PBS for 30 min. For subsequent immunolabelling with anti-D, tissues were immersed in methanol (−20°C) for 3 to 5 min. The tissues were preincubated in PBS containing 20% goat serum for 1 hour at room temperature, prior to overnight incubation with the anti-stereocilin antibodies (~1 μg/ml) in PBS containing 1% bovine serumalbumine (PBS/BSA). Whole mount preparations were analysed with a laser scanning confocal microscope (LSM-510, Zeiss). Immunolabelling for SEM was done as for immunofluorescence detection. Primary antibodies were detected with protein A-conjugated 15 nm colloidal gold particles (EM Lab, Utrecht, The Netherlands; diluted 1/60 in PBS/BSA). Finally, samples were post-fixed for 1 hour in 2.5% glutaraldehyde in PBS before proceeding to SEM.

References

31. Kress C, Vandormael-Pournin S, Baldacci P, Cohen-Tannoudji M, Babinet C. Nonpermissiveness for mouse embryonic stem (ES) cell derivation circumvented by a single backcross to 129/Sv strain: establishment of ES cell lines bearing the Omd conditional lethal mutation. Mamm. Genome. 1998; 9:998–1001. [PubMed: 9880667]

32. Lallemand Y, Luria V, Haffner-Krausz R, Lonai P. Maternally expressed PGK-Cre transgene as a tool for early and uniform activation of the Cre site-specific recombinase. Transgenic Res. 1998; 7:105–112. [PubMed: 9608738]
33. Michel V, et al. Cadherin 23 is a component of the transient lateral links in the developing hair bundles of cochlear sensory cells. Dev. Biol. 2005; 280:281–294. [PubMed: 15882573]
34. Delmaghani S, et al. Mutations in the gene encoding pejvakin, a newly identified protein of the afferent auditory pathway, cause DFNB59 auditory neuropathy. Nat. Genet. 2006; 38:770–778. [PubMed: 16804542]

Scanning electron microscopy

Samples were processed as described[34]. When immunolabelling was coupled to SEM, dried specimens were mounted on colloidal silver adhesive (Quick drying silver paint, Agar Scientific) to enhance their conductivity. Specimens were then coated with 30 nm of carbon and imaged using a Yttrium Aluminium Garnet (YAG) detector.

Transmission electron microscopy

For immunogold electron microscopy, pre-embedding labelling using the anti-B antibody was done as described[33]. Procedures for transmission electron microscopy were as described[7].

Supplementary Material

Refer to Web version on PubMed Central for supplementary material.

Acknowledgments

We thank M. Lenoir, S. Guadagnini and M.-C. Prévost for advice on scanning electron microscopy, E. Perret and P. Roux for advice on confocal microscopy, S. Chardenoux, S. Nouaille and A. Mallet for technical help, Y. Lallemand for providing us with PGK-Cre^{m} mice, N. Michalski for help with figure drawing and J. Boutet de Monvel for critical reading of the manuscript. This work was supported by the European Commission FP6 Integrated Project EuroHear, Fondation Raymonde et Guy Strittmatter, Région Ile-de-France (Programme Sésame), and the Wellcome Trust.

REFERENCES

1. Goldstein JL. Auditory nonlinearity. J. Acoust. Soc. Am. 1967; 41:676–689. [PubMed: 6045077]
2. Delgutte, B. Physiological models for basic auditory percepts. In: Hawkins, HH.; McMullen, TA.; Popper, AN.; Fay, RR., editors. Auditory Computation. Springer; New York: 1996. p. 157-220.
3. Kemp DT. Stimulated acoustic emissions from within the human auditory system. J. Acoust. Soc. Am. 1978; 64:1386–1391. [PubMed: 744838]
4. Verpy E, et al. Mutations in a new gene encoding a protein of the hair bundle cause non-syndromic deafness at the DFNB16 locus. Nat. Genet. 2001; 29:345–349. [PubMed: 11687802]
5. Furness DN, Hackney CM. Cross-links between stereocilia in the guinea pig cochlea. Hear. Res. 1985; 18:177–188. [PubMed: 4044419]
6. Tsuprun V, Santi P. Structure of outer hair cell stereocilia side and attachment links in the chinchilla cochlea. J. Histochem. Cytochem. 2002; 50:493–502. [PubMed: 11897802]
7. Goodyear RJ, Marcotti W, Kros CJ, Richardson GP. Development and properties of stereociliary link types in hair cells of the mouse cochlea. J. Comp. Neurol. 2005; 485:75–85. [PubMed: 15776440]
8. Brownell WE, Bader CR, Bertrand D, de Ribaupierre Y. Evoked mechanical responses of isolated cochlear outer hair cells. Science. 1985; 227:194–196. [PubMed: 3966153]
9. Ashmore JF. A fast motile response in guinea-pig outer hair cells: the cellular basis of the cochlear amplifier. J. Physiol. 1987; 388:323–347. [PubMed: 3656195]

10. He DZ, Dallos P. Somatic stiffness of cochlear outer hair cells is voltage-dependent. Proc. Natl. Acad. Sci. USA. 1999; 96:8223–8228. [PubMed: 10393976]
11. Liberman MC, et al. Prestin is required for electromotility of the outer hair cell and for the cochlear amplifier. Nature. 2002; 419:300–304. [PubMed: 12239568]
12. Hudspeth AJ. How the ear's works work. Nature. 1989; 341:397–404. [PubMed: 2677742]
13. Kennedy HJ, Crawford AC, Fettiplace R. Force generation by mammalian hair bundles supports a role in cochlear amplification. Nature. 2005; 433:880–883. [PubMed: 15696193]
14. Dallos P, Harris D. Properties of auditory nerve responses in absence of outer hair cells. J. Neurophysiol. 1978; 41:365–383. [PubMed: 650272]
15. Liberman MC, Dodds LW. Single-neuron labeling and chronic cochlear pathology. III. Stereocilia damage and alterations of threshold tuning curves. Hear. Res. 1984; 16:55–74. [PubMed: 6511673]
16. Robles L, Ruggero MA. Mechanics of the mammalian cochlea. Physiol. Rev. 2001; 81:1305–1352. [PubMed: 11427697]
17. Patuzzi RB, Yates GK, Johnstone BM. Outer hair cell receptor current and sensorineural hearing loss. Hear. Res. 1989; 42:47–72. [PubMed: 2684949]
18. Dallos P, Cheatham MA. Compound action potential (AP) tuning curves. J. Acoust. Soc. Am. 1976; 59:591–597. [PubMed: 1254787]
19. Moore, BCJ. Cochlear hearing loss. Whurr Publishers Ltd; London: 1998.
20. Ruggero MA, Robles L, Rich NC. Two-tone suppression in the basilar membrane of the cochlea: mechanical basis of auditory-nerve rate suppression. J. Neurophysiol. 1992; 68:1087–1099. [PubMed: 1432070]
21. Kim DO, Molnar CE, Matthews JW. Cochlear mechanics: nonlinear behavior in two-tone responses as reflected in cochlear-nerve-fiber responses and in ear-canal sound pressure. J. Acoust. Soc. Am. 1980; 67:1704–1721. [PubMed: 7372925]
22. Robles L, Ruggero MA, Rich NC. Two-tone distortion on the basilar membrane of the chinchilla cochlea. J. Neurophysiol. 1997; 77:2385–2399. [PubMed: 9163365]
23. Kimura RS. Hairs of the cochlear sensory cells and their attachment to the tectorial membrane. Acta Otolaryngol. 1966; 61:55–72. [PubMed: 5331578]
24. Legan PK, et al. A targeted deletion in alpha-tectorin reveals that the tectorial membrane is required for the gain and timing of cochlear feedback. Neuron. 2000; 28:273–285. [PubMed: 11087000]
25. Lukashkin AN, Lukashkina VA, Legan PK, Richardson GP, Russell IJ. Role of the tectorial membrane revealed by otoacoustic emissions recorded from wild-type and transgenic Tecta(deltaENT/deltaENT) mice. J. Neurophysiol. 2004; 91:163–171. [PubMed: 14523068]
26. Patuzzi, R. Cochlear micromechanics and macromechanics. In: Dallos, P.; Popper, AN.; Fay, RR., editors. The cochlea. Springer; New York: 1996. p. 186-257.
27. van Netten SM, Kros CJ. Gating energies and forces of the mammalian hair cell transducer channel and related hair bundle mechanics. Proc. Biol. Sci. 2000; 267:1915–1923. [PubMed: 11052545]
28. Howard J, Hudspeth AJ. Compliance of the hair bundle associated with gating of mechanoelectrical transduction channels in the bullfrog's saccular hair cell. Neuron. 1988; 1:189–199. [PubMed: 2483095]
29. Flock A, Strelioff D. Graded and nonlinear mechanical properties of sensory hairs in the mammalian hearing organ. Nature. 1984; 310:597–599. [PubMed: 6462248]
30. Fettiplace R. Active hair bundle movements in auditory hair cells. J. Physiol. 2006; 576:29–36. [PubMed: 16887874]

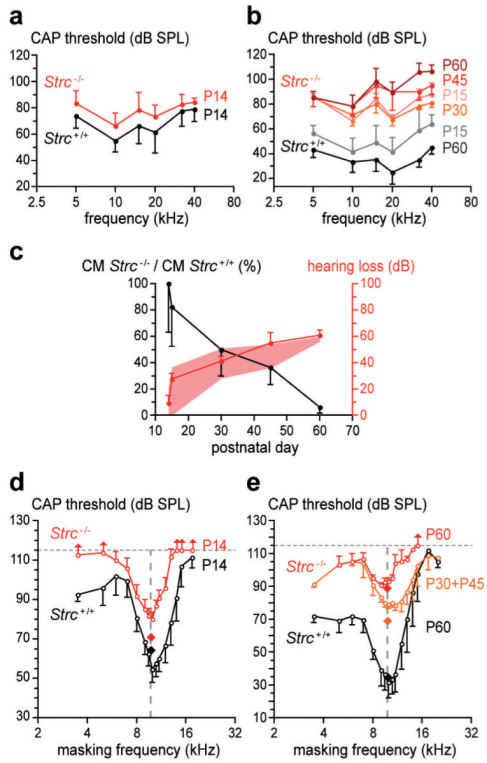

Figure 1. Hearing sensitivity and frequency tuning in stereocilin-null versus wild-type mice

(**a**) Mean CAP thresholds (±sd; n=7) in P14 mice. The difference between *Strc*$^{+/+}$ and *Strc*$^{-/-}$ mice is non-significant (p>0.05). (**b**) Mean CAP thresholds (±sd; n=5) in P15 to P60 mice. (**c**) Ratio of CM amplitudes in *Strc*$^{-/-}$ vs *Strc*$^{+/+}$ mice at low frequencies (black curve), with predicted (pink shading) and actual (red curve) hearing loss. Differences, predicted vs actual, are non-significant (p>0.05). (**d**) CAP tuning curves in P14 mice (±sd; n=7). $Q_{10\ dB}$ (ratio of test frequency to CAP tuning curve width at 10 dB above its tip) is similar in *Strc*$^{-/-}$ ($Q_{10\ dB}$ = 3.1) and *Strc*$^{+/+}$ ($Q_{10\ dB}$ = 3.2) mice. (**e**) CAP tuning curves (±sd) in P60 *Strc*$^{+/+}$ mice ($Q_{10\ dB}$ = 3.4, n=5) and *Strc*$^{-/-}$ mice (P30 + P45, $Q_{10\ dB}$ = 2.2, n=4; P60, $Q_{10\ dB}$ = 3.1, n=4). Diamonds indicate test-tone levels. Vertical arrows indicate lack of masking in some animals for a masking-tone level of 115 dB SPL.

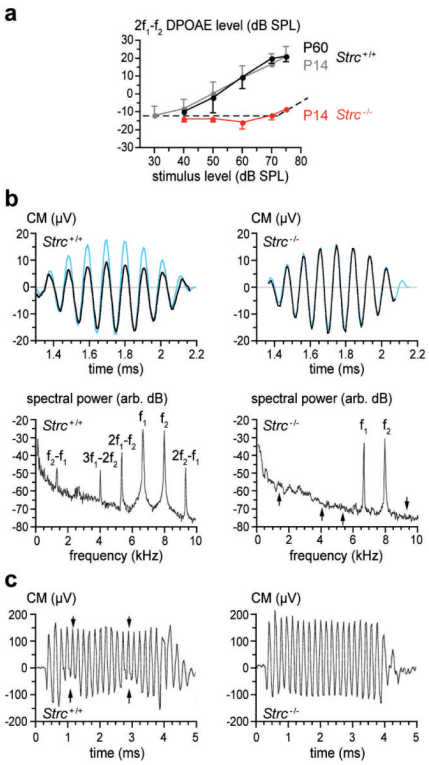

Figure 2. Waveform distortions in wild-type and stereocilin-null mice

(**a**) DPOAE amplitude (mean ±sd) at frequency $2f_1$-f_2 as a function of sound pressure level common to stimuli f_1 and f_2 (f_2/f_1 = 1.20) in *Strc*$^{+/+}$ (P14, P60) and *Strc*$^{-/-}$ (P14) mice (n=8). Dotted line: noise floor. (**b**) Temporal waveforms and frequency spectra (black lines) of the CM in P14 mice, in response to one cycle of the beat of a pair of pure-tone stimuli (6.7 and 8 kHz, 65 dB SPL each, blue traces in upper panels, scaled to the CM response of the *Strc*$^{+/+}$ ear). Arrows in *Strc*$^{-/-}$ CM frequency spectrum mark positions of intermodulation frequencies. (**c**) Amplitude modulation (arrows) of the CM response to a 5 kHz, 70 dB tone-burst by two periods of a 95 dB SPL infrasound (550 Hz), in P14 mice.

Europe PMC Funders Author Manuscripts

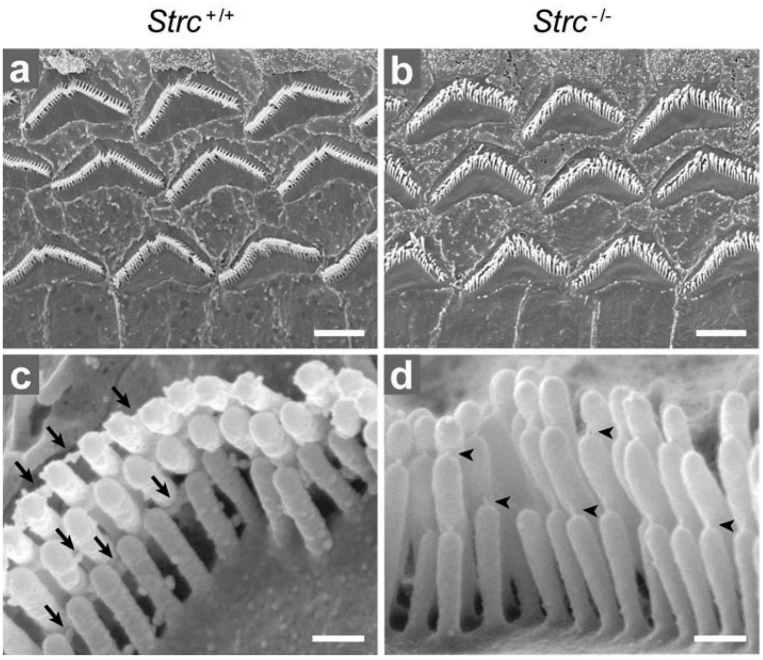

Figure 3. OHC hair bundle morphology in P14 wild-type and stereocilin-null mice

(**a, b**) Low-magnification scanning electron micrographs showing the three rows of OHCs. The tops of stereocilia are less clearly aligned in the *Strc*$^{-/-}$ mouse (**b**) than in the *Strc*$^{+/+}$ mouse (**a**). (**c, d**) Detailed views of single OHC hair bundles. Top connectors (arrows in c) are not detected in the *Strc*$^{-/-}$ mouse, while tip links (arrowheads in d) are present. Scale bars: 2.5 μm (a, b), 0.25 μm (c, d).

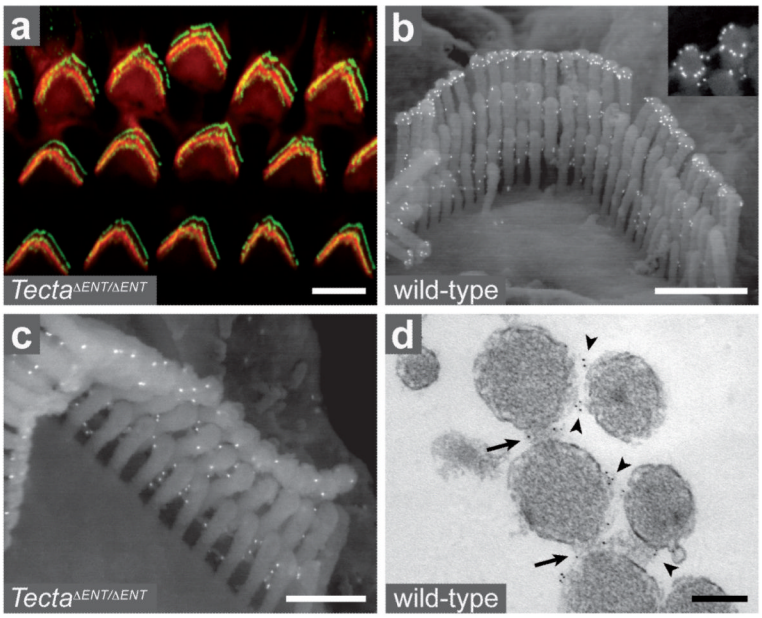

Figure 4. Immunodetection of stereocilin in wild-type and *Tecta*$^{\Delta ENT/\Delta ENT}$ OHCs

(**a**) Confocal image of *Tecta*$^{\Delta ENT/\Delta ENT}$ OHC hair bundles (P14) stained for stereocilin (green) and actin (red). (**b, c**) Immunogold scanning electron micrographs of wild-type and *Tecta*$^{\Delta ENT/\Delta ENT}$ OHC hair bundles (P14) labelled for stereocilin. A ring-shaped labelling is seen around the tip of the tallest stereocilia in wild-type (b, **inset**) but not *Tecta*$^{\Delta ENT/\Delta ENT}$ mice (c). In contrast, the labelling between stereocilia is seen both in the wild-type and *Tecta*$^{\Delta ENT/\Delta ENT}$ mice. (**d**) Transmission electron micrograph of a stereocilin-labelled OHC hair bundle (P22, transverse section). Top connectors within (arrows) and between (arrowheads) rows are labelled. Scale bars: 5 μm (a), 1 μm (b), 0.5 μm (c), 0.2 μm (d).